

OLCI Level 2

Algorithm Theoretical Basis Document

Glint Correction

DOCUMENT REF: S3-L2-SD-03-C09-ARG-ATBD
DELIVERABLE REF: SD-03-C
VERSION: 2.1
DATE: 11-10-2012

	<p style="text-align: center;">SENTINEL-3 OPTICAL PRODUCTS AND ALGORITHM DEFINITION</p> <p style="text-align: center;">OLCI Level 2 ATBD Glint Correction</p>	<p>Ref: S3-L2-SD-03-C09-ARG- ATBD Issue: 2.1 Date: 11/10/2012 Page 2 of 24</p>
---	--	--

Document Signature Table

	Name	Function	Company	Signature	Date
Prepared	S. Lavender S. Kay	Project Manager PhD Student	ARGANS		
Verified	O. Fanton d'Andon	OLCI Coordinator	ACRI-ST		
Released	S. Emsley	Project Manager	ARGANS		11-10-2012

Change record

Issue	Date	Description	Change pages
1.0	27/08/2009	Version 1 (PDR delivery)	
2.0	08/04/2010	Version 2 (CDR delivery)	Updated typos in equation 4; enhanced error analysis and minor modifications to the other sections
2.1	11/10/2012	Version 2.1 (FR delivery)	Put The baseline implementation at start of 3.1 [S3OPTL2PADCDR-161]

	<p align="center">SENTINEL-3 OPTICAL PRODUCTS AND ALGORITHM DEFINITION</p> <p align="center">OLCI Level 2 ATBD Glint Correction</p>	<p>Ref: S3-L2-SD-03-C09-ARG- ATBD Issue: 2.1 Date: 11/10/2012 Page 3 of 24</p>
---	--	--

Distribution List

Organisation	To	Nb. of copies
ESA	P. Goryl	
EUMETSAT	Hilary Wilson, Anne O'Carroll	
S3 Optical team	All OLCI team	

Table of Contents

1.	INTRODUCTION	6
1.1	Acronyms and Abbreviations.....	6
1.2	Symbols.....	6
1.3	Purpose and Scope.....	7
1.4	Algorithm Identification	7
2.	ALGORITHM OVERVIEW.....	8
2.1	Objectives.....	8
3.	ALGORITHM DESCRIPTION	10
3.1	Theoretical Description.....	10
3.2	Algorithm Validation	11
3.1	Error Budget.....	13
4.	PRACTICAL CONSIDERATIONS / EVOLUTION	19
6.	ASSUMPTIONS AND LIMITATIONS	21
7.	INPUT DATA	21
8.	REFERENCES.....	22
	ACKNOWLEDGEMENTS.....	24

List of Figures

Figure 1: (a) Sub-set of a MERIS image from the Pacific Ocean and (b) Sensor radiance plotted for 4 wavebands along the line marked in (a). Modified from Kay et al. (2009). 12

Figure 2: SeaWiFS image showing sun glint in the Indian Ocean, near the Horn of Africa. (a) quasi true colour image (b) the calculated glint radiance (c) masks over the moderate (mauve) and high (pink) glint areas. 13

Figure 3: Percentage change in top of atmosphere glint reflectance for a 5% change in each input variable. 14

Figure 4: Section of a MERIS image of the Pacific Ocean, showing the position of 6 pixels A-F. (a) level 1 RGB image (b) level 2 image with sun glint flag. 15

Figure 5: Top of atmosphere glint reflectance calculated with each input varying randomly about its reported value (results from 1000 runs). 16

Figure 6: Top of atmosphere glint reflectance calculated for values across the full range of all input variables, plotted against each variable. Note that points with values of glint reflectance above 10 are not shown. 18

Figure 7: Top of atmosphere glint reflectance calculated for values across the full range of all input variables, plotted against each variable using the Gaussian PDF version of the glint function. 18

Figure 8: CASI imagery for the 13 June 2003 flown over the Tamar Estuary and Plymouth Sound, UK. The quasi true coloured images (a and c) represent composites of wavebands centred at 672, 561 and 491 nm as red, green and blue. From left to right the images are uncorrected image, non-water mask, aerosol corrected image and TSM product with the scale bar. 20

List of Tables

Table 1 Glint reflectance and uncertainty produced by a 5% change in wind speed for the 6 pixels shown in Fig 2. Atmospheric transmittance has been taken as 1. 15

Table 2 Mean glint reflectance and standard deviation when each input is varied randomly about its reported value (results from 1000 runs). All inputs were varied in a normal distribution with a standard deviation of 5% of the reported value. Atmospheric transmittance has been taken as 1. 16

1. INTRODUCTION

1.1 Acronyms and Abbreviations

AC	Atmospheric Correction
ATBD	Algorithm Theoretical Basis Document
CASI	Compact Airborne Spectrographic Imager
ECMWF	European Centre for Medium-Range Weather Forecasts
FOV	Field-Of-View
GLI	Global Imager
MERIS	Medium Resolution Imaging Spectrometer
MODIS	Moderate Resolution Imager
NCEP	National Centers for Environmental Protection
NERC	Natural Environment Research Council
NN	Neural Network
OLCI	Ocean Land Colour Imager
OZA	Operating Zenith Angle
PDF	Probability Distribution Function
RT	Radiative Transfer
SeaWiFS	Sea-viewing Field-of-view Spectrometer
TOA	Top Of Atmosphere
TSM	Total Suspended Matter

1.2 Symbols

Symbol	definition	Dimension / units
Geometry, wavelengths		
λ	Wavelength	nm
θ_s	Sun zenith angle ($\mu_s = \cos(\theta_s)$)	degrees
θ_v	Satellite viewing angle ($\mu_v = \cos(\theta_v)$)	degrees
$\Delta\phi$	Azimuth difference between the sun-pixel and pixel-sensor half vertical planes	degrees
Atmosphere and aerosol properties		
$t_d(\lambda, \theta)$	Diffuse transmittance for angle θ	dimensionless
	$t_d(\lambda, \theta) = L_-(\lambda, \theta_s, \theta_v, \Delta\phi) / L_{0+}(\lambda, \theta_s, \theta_v, \Delta\phi)$	
$\rho(\lambda, \theta_s, \theta_v, \Delta\phi)$	Reflectance ($\pi L / F_0 \mu_s$)	dimensionless

where the product $\pi.L$ is the TOA upwelling irradiance if upwelling radiances are equal to $L(\lambda, \theta_s, \theta_v, \Delta\phi)$, for any values of θ_v within $0-\pi/2$ and any $\Delta\phi$ within $0-2\pi$.

Subscripts are

- t: total reflectance
- w: water-leaving reflectance
- g: sun glint reflectance

Water properties

$[\rho_w]_N(\lambda)$ Normalised water-leaving reflectance (*i.e.*, the reflectance if there were no atmosphere, and for $\theta_s = \theta_v = 0$)
 dimensionless

Air-water interface

$\rho_F(\theta)$ is the Fresnel reflection coefficient for incident angle θ
 dimensionless

σ Root-mean square of wave facet slopes
 dimensionless

β Angle between the local normal and the normal to a wave facet

p Probability density of surface slopes for the direction $(\theta_s, \theta_v, \Delta\phi)$
 dimensionless

Miscellaneous

W Wind speed
 dimensionless

1.3 Purpose and Scope

Sun glint is an issue for ocean colour imagery as it can lead to an inaccurate retrieval of atmospheric products (Wang & Bailey, 2001) if it isn't masked and/or corrected for. For example, sun glint currently cancels almost half of Medium Resolution Imaging Spectrometer (MERIS) observation at sub-tropical latitudes (Steinmetz et al., 2008). This ATBD discusses the potential approaches to correct sun glint for OLCI. The amount of sun glint will be reduced as compared to MERIS; the field-of-view (FOV) is tilted to reduce the sun-glint pollution (maximum Operating Zenith Angle, OZA, of 55°).

1.4 Algorithm Identification

This algorithm is identified under reference "SD-03-C09" in the Sentinel-3 OLCI documentation.

	<p style="text-align: center;">SENTINEL-3 OPTICAL PRODUCTS AND ALGORITHM DEFINITION</p> <p style="text-align: center;">OLCI Level 2 ATBD Glint Correction</p>	<p>Ref: S3-L2-SD-03-C09-ARG- ATBD Issue: 2.1 Date: 11/10/2012 Page 8 of 24</p>
---	--	--

2. ALGORITHM OVERVIEW

2.1 Objectives

For given positions of the sun and the satellite, there is only one slope and orientation of the water surface that will reflect incident sun light into the measuring instrument. The glint pattern is made up of many point sources, each a reflection from a point on the water surface oriented correctly to reflect incident light directly to the sensor. With ocean colour sensors, pixels of around 500m in size, the individual glint sources cannot be identified and the glint and non-glint signal is averaged within a pixel. Therefore, the aim of the glint correction is to identify and subtract the contribution of the glint reflectance, ρ_g , to the top of atmosphere (TOA) reflectance, ρ_t .

In the 1950s, Cox and Munk studied the link between sun glint and the wind-driven waves on the sea surface (Cox & Munk, 1954a; Cox & Munk, 1954b; Cox & Munk, 1956). In the last decade several studies have repeated the method of Cox and Munk, but using much larger data sets from satellite-borne radiometers and scatterometers able to gather concurrent radiance and wind data. Ebuchi & Kizu (2002) used about 30 million data points gathered over 4 years' observation of subtropical seas and found that the distribution of slopes was narrower than the Cox and Munk model and the dependence on wave direction was weaker. The accuracy of the Cox and Munk model was also supported by Fox et al. (2007), who used satellite glint patterns to assess wind speed and compared this with data from buoys. Fukushima et al. (2009) carried out a similar study using radiance data from GLI imagery and concurrent wind data from the SeaWinds scatterometer on the same satellite. They found good agreement with Cox and Munk for moderate wind speeds, but the model of Ebuchi and Kizu was a better fit in calm conditions. This difference in response at lower wind speed is also supported by Wu's (1990) reanalysis of the Cox and Munk data. The study of Gatebe et al. (2005), using data from airborne instruments for the western Atlantic Ocean, also found that the Cox and Munk model fitted their data well for most conditions, but underestimated the glint at the centre of the pattern; i.e. wind speeds below 3 m/s.

For both SeaWiFS (which tilts to reduce glint contamination) and MERIS (no tilt) the glint is predicted from wind speed and subtracted where it falls between two thresholds (Wang & Bailey, 2001; Wang et al. 2002; Montagner et al., 2003). The glint and aerosol are estimated together. It is based Cox and Munk sea surface model and so neglects local wind conditions (the wind data is from coarse resolution model outputs, NCEP and ECMWF). For GLI, Fukushima et al. (2007) used a similar approach as for SeaWiFS, but with wind speed

	<p style="text-align: center;">SENTINEL-3 OPTICAL PRODUCTS AND ALGORITHM DEFINITION</p> <p style="text-align: center;">OLCI Level 2 ATBD Glint Correction</p>	<p>Ref: S3-L2-SD-03-C09-ARG- ATBD Issue: 2.1 Date: 11/10/2012 Page 9 of 24</p>
---	--	--

from the SeaWinds microwave scatterometer on the same satellite (ADEOSII). Ottaviani et al. (2008) also uses the Cox and Munk model, but with a full radiative transfer (RT) solution that includes the effect of multiple scattering, multiple reflection and shadowing. Steinmetz et al. (2008) corrects MERIS for aerosol and glint together by matching reflectance using a neural network or iterative mean square minimization method.

	SENTINEL-3 OPTICAL PRODUCTS AND ALGORITHM DEFINITION OLCI Level 2 ATBD Glint Correction	Ref: S3-L2-SD-03-C09-ARG- ATBD Issue: 2.1 Date: 11/10/2012 Page 10 of 24
---	--	---

3. ALGORITHM DESCRIPTION

3.1 Theoretical Description

The **baseline implementation** is based on the evolution of the Montagner et al (2003) MERIS approach. Alternative approaches could have been Steinmetz et al. (2008), which is called POLYMER, and the Doerffer et al. (2008) Neural Network (NN). A NN approach combined into an atmospheric correction (AC) has been included through ATBD SD-03-C17 termed the “alternative atmospheric correction”.

MERIS Approach

For MERIS, all water pixels are tested for glint by comparing the reflectance to the predicted glint reflectance (ACRI, 2006):

$$\rho_g = \frac{\pi \rho(\omega) \rho(\xi, \eta)}{4 \cos \theta_s \cos \theta_v \cos^4 \beta} \quad (\text{Eq 1})$$

Where $\rho(\omega)$ is the Fresnel reflectance (approximated as a constant, 0.02, for incidence angles between 0 and 50 degrees), $\rho(\xi, \eta)$ is the probability distribution function (PDF) for the sea surface slope and β is the zenith angle of the wave facet calculated from the specular reflection angle (ω), see equation 2.

$$\cos 2\omega = \cos \theta_s \cos \theta_v + \sin \theta_s \sin \theta_v \cos(\Delta\phi) \quad (\text{Eq 2})$$

$$\cos \beta = \frac{\cos \theta_s + \cos \theta_v}{(2 + 2 \cos 2\omega)^{1/2}} \quad (\text{Eq 3})$$

$$p(\xi, \eta) = \frac{1}{2\pi\sigma_u\sigma_c} e^{-\frac{\xi^2 + \eta^2}{2}} \left[1 - \left(\frac{1}{2}\right) C_{221} \eta (\xi^2 - 1) - \left(\frac{1}{6}\right) C_{03} (\eta^3 - 3\eta) + \left(\frac{1}{24}\right) C_{40} (\xi^4 - 6\xi^2 + 3) + \left(\frac{1}{4}\right) C_{222} (\xi^2 - 1)(\eta^2 - 1) + \left(\frac{1}{24}\right) C_{04} (\eta^4 - 6\eta^2 + 3) \right] \quad (\text{Eq 4})$$

$$\sigma_c = (\sigma_c^0 + \sigma_c^1 W)^{1/2} \quad (\text{Eq 5})$$

	SENTINEL-3 OPTICAL PRODUCTS AND ALGORITHM DEFINITION OLCI Level 2 ATBD Glint Correction	Ref: S3-L2-SD-03-C09-ARG- ATBD Issue: 2.1 Date: 11/10/2012 Page 11 of 24
---	--	---

$$\sigma_u = (\sigma_u^0 + \sigma_u^1 W)^{1/2} \quad (\text{Eq 6})$$

$$\xi = \frac{1}{\sigma_c} z'_x \quad (\text{Eq 7})$$

$$\eta = \frac{1}{\sigma_u} z'_y \quad (\text{Eq 8})$$

$$z'_x = \cos(\chi) z_x + \sin(\chi) z_y \quad (\text{Eq 9})$$

$$z'_y = -\sin(\chi) z_x + \cos(\chi) z_y \quad (\text{Eq 10})$$

$$z_x = \frac{-\sin\theta_v \sin\Delta\phi}{\cos\theta_s + \cos\theta_v} \quad (\text{Eq 11})$$

$$z_y = \frac{\sin\theta_v \cos\Delta\phi + \sin\theta_s}{\cos\theta_s + \cos\theta_v} \quad (\text{Eq 12})$$

Where χ is the wind direction in the local frame (clockwise from the sun), $\sigma_c^0 = 0.003$, $\sigma_c^1 = 1.92 \times 10^{-3}$, $\sigma_u^0 = 0.000$, $\sigma_u^1 = 3.16 \times 10^{-3}$, $C_{21} = C_{21}^0 + C_{21}^1 W$, $C_{21}^0 = 0.01$, $C_{21}^1 = -0.0086$, $C_{22} = 0.12$, $C_{03} = C_{03}^0 + C_{03}^1 W$, $C_{03}^0 = 0.04$, $C_{03}^1 = -0.033$, $C_{40} = 0.40$, $C_{04} = 0.23$ and W is the windspeed [m/s].

The glint reflectance is then converted to a TOA reflectance using a diffuse atmospheric transmittance that includes Rayleigh scattering and ozone, but not aerosol. For medium glint reflectance the pixel is corrected by subtracting the glint. Low glint values are not adjusted, to avoid over-correction given the uncertainty in the wind data and Cox and Munk model – the threshold is set at the lowest level where glint is found to affect the atmospheric correction. High levels, where the glint reflectance at 865 nm is more than 80% of the observed reflectance, are flagged and not processed further – for these values glint is significantly affecting the aerosol retrieval and correction is not possible. Atmospheric correction, including aerosol, is done at a later stage of level 2 processing.

3.2 Algorithm Validation

Figure 1 (a) is a MERIS image from the Pacific Ocean with sun glint on the right hand side. The spectral shape of the glint contaminated pixels, Figure 1(b), is that the TOA radiance increases in all bands, but with a greater slope in the near infra-red.

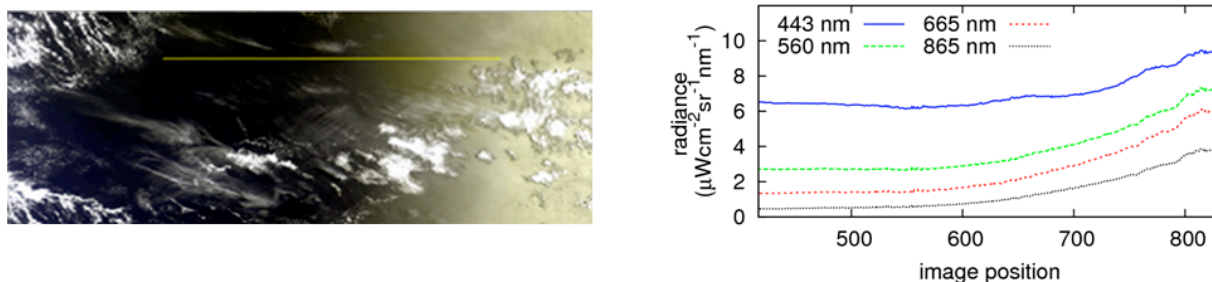
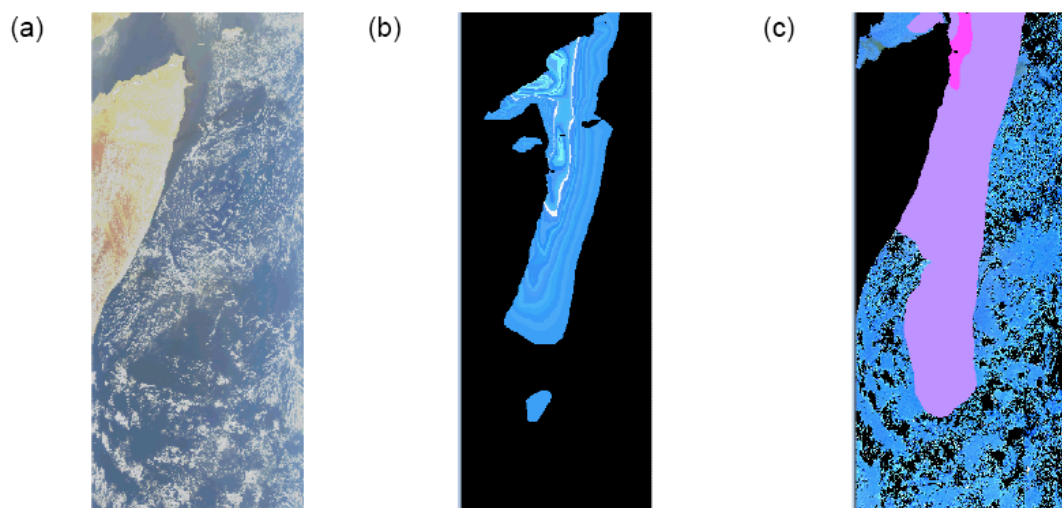


Figure 1: (a) Sub-set of a MERIS image from the Pacific Ocean and (b) Sensor radiance plotted for 4 wavebands along the line marked in (a). Modified from Kay et al. (2009).

Figure 2 shows the glint correction as implemented in the SeaDAS package as part of the MSL12 (Multi-Sensor Level 1 to Level 2) code. This code takes as input Level 1a data, consisting of raw radiances, along with navigational and instrument information. The output level 2 data includes the glint radiance (normalised) as well as normalised water-leaving radiances for each band, corrected for glint where possible. The threshold for glint flagging and correction can be chosen. The maximum number of iterations for the glint/aerosol calculation can also be set, the default is 10.

The global coverage of the study by Bréon and Henriot (2006) gives some confidence in the use of the Cox and Munk model for a wide variety of sea states.



	<p style="text-align: center;">SENTINEL-3 OPTICAL PRODUCTS AND ALGORITHM DEFINITION</p> <p style="text-align: center;">OLCI Level 2 ATBD Glint Correction</p>	<p>Ref: S3-L2-SD-03-C09-ARG- ATBD Issue: 2.1 Date: 11/10/2012 Page 13 of 24</p>
---	--	---

Figure 2: SeaWiFS image showing sun glint in the Indian Ocean, near the Horn of Africa. (a) quasi true colour image (b) the calculated glint radiance (c) masks over the moderate (mauve) and high (pink) glint areas.

3.1 Error Budget

An error model will (ideally) be based on probability density functions (PDFs) provided for the input variables (θ_s , θ_v , $\Delta\phi$, t_d and W), which will be propagated through the sun glint equations (model) to obtain an output PDF. An alternative is a sensitivity analysis where the input variables are varied by $\pm 5\%$ and the variation in the output analysed.

As input variable PDFs aren't currently available, current research has focused on the sensitivity analysis. The predicted glint radiance is non-linear in all input variables except the atmospheric transmittance, which itself is a function of the illumination and viewing geometries. Therefore, the calculated radiance is highly sensitive to changes in the input variables in at least part of their ranges. This can be demonstrated by evaluating how the glint function changes as a result of a 5% change in each input variable, using values from across the full range of all variables ([Figure 3](#)) (Saltelli et al. 2006).

[Figure 4](#) and [Table 1](#) show an example of sensitivity estimation for 6 pixels in a MERIS image. In this case the wind speed has been varied by 5% and the corresponding change in glint reflectance is shown. The high percentage uncertainties in the low glint region will not impact on the final uncertainty as these reflectances are too low to be considered as medium glint. However, the uncertainty at pixel C will lead to uncertainty in the corrected reflectance and the uncertainty at D could change the classification of the pixel as high/medium glint.

This illustrates how uncertainty in the calculated glint radiance can lead to two types of error:

- Uncertainty in the size of the corrected radiance for the medium glint region (e.g. pixel C in Fig 2). This will lead to an uncertainty that propagates along the downstream processing chain.
- A pixel can be wrongly categorised as low, medium or high glint (e.g. pixel D in Fig 2). This is more difficult to quantify at later stages of processing, but can at least be reported to the user.

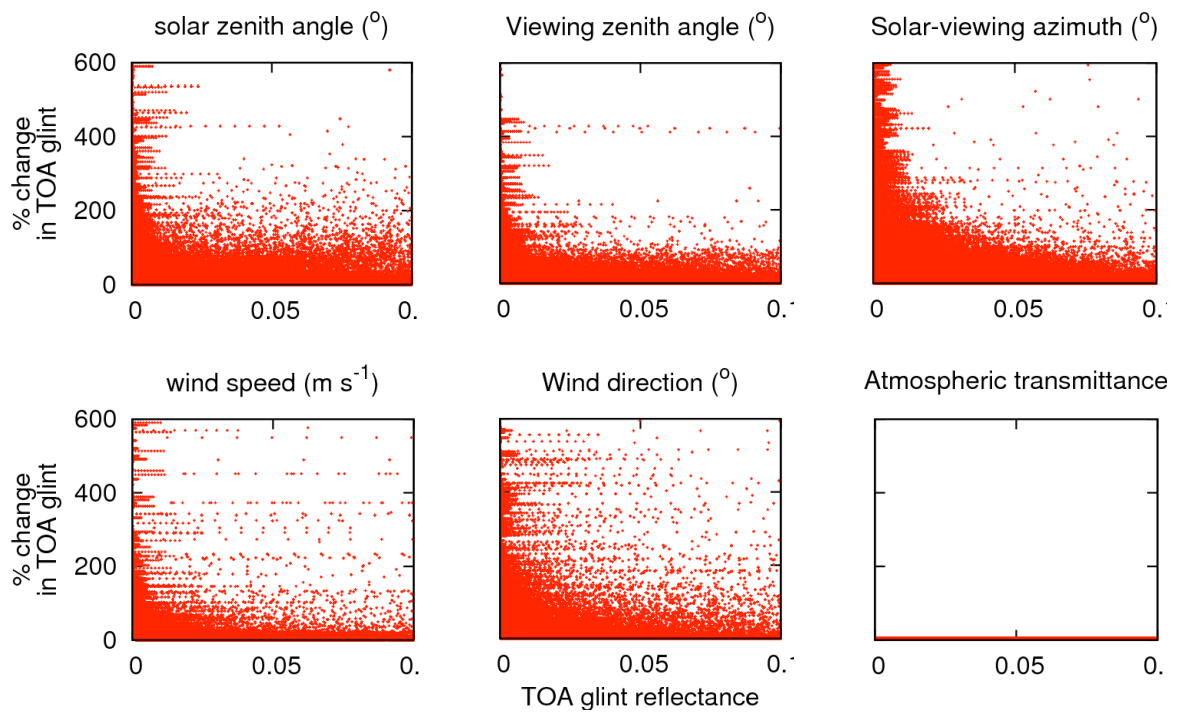


Figure 3: Percentage change in top of atmosphere glint reflectance for a 5% change in each input variable.

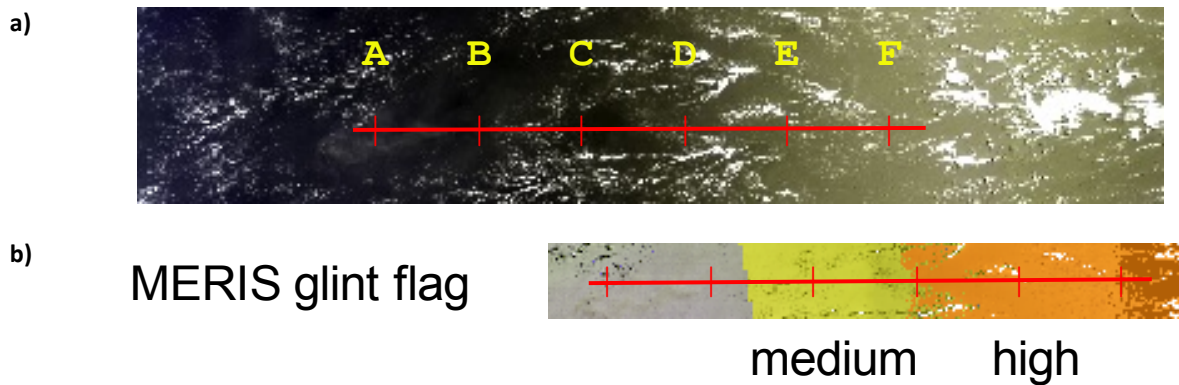


Figure 4: Section of a MERIS image of the Pacific Ocean, showing the position of 6 pixels A-F. (a) level 1 RGB image (b) level 2 image with sun glint flag.

Table 1 Glint reflectance and uncertainty produced by a 5% change in wind speed for the 6 pixels shown in Fig 2. Atmospheric transmittance has been taken as 1.

Position	Glint flag	TOA glint reflectance	Absolute uncertainty	Relative uncertainty (%)
A	none	1.60×10^{-7}	6.75×10^{-7}	420
B	none	0.0006	0.00062	101
C	medium	0.0185	0.00282	15
D	high	0.0327	0.00175	5.4
E	high	0.0547	0.00005	0.1
F	high	0.0777	0.00179	2.3

To estimate the uncertainty in the glint reflectance at a given pixel, the calculation can be re-run with all inputs varying randomly around their reported values, with a distribution in line with the uncertainty reported in the level 1 data. An example is shown in [Figure 5](#) for the 6 pixels in [Figure 4](#). All inputs have been varied randomly in a normal distribution with a standard deviation of 5% of their measured value – in practice the distribution used should be based in knowledge of the distribution of uncertainties in the input data (Helton et al. 2006).

For each pixel, the standard deviation of the calculated reflectances can be reported as the uncertainty ([Table 2](#)). The mean value for TOA glint reflectance is given, rather than the value calculated from the reported input values: as long as enough repeat runs have been done the difference should be small. As before, the high uncertainties in the low glint region (pixels A and B) would not impact on the final uncertainty.

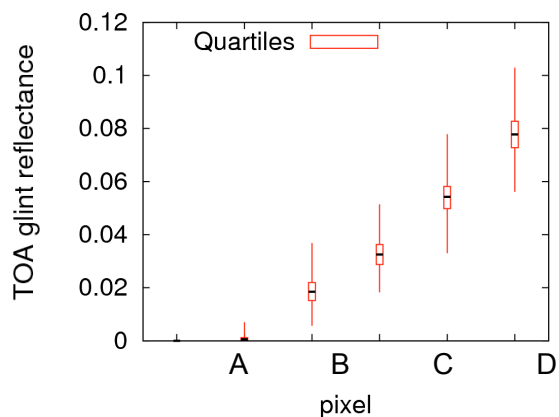


Figure 5: Top of atmosphere glint reflectance calculated with each input varying randomly about its reported value (results from 1000 runs).

Table 2 Mean glint reflectance and standard deviation when each input is varied randomly about its reported value (results from 1000 runs). All inputs were varied in a normal distribution with a standard deviation of 5% of the reported value. Atmospheric transmittance has been taken as 1.

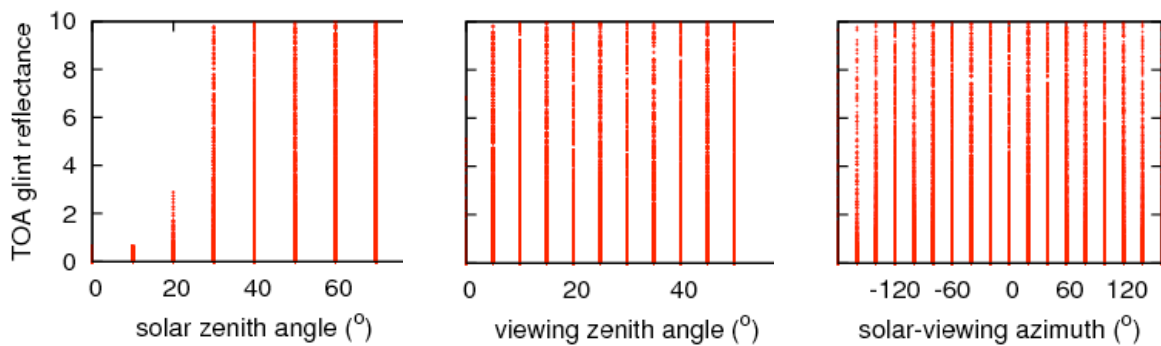
Position	Mean TOA glint reflectance	Standard deviation	Standard deviation as % of TOA glint reflectance
A	3.23×10^{-6}	1.39×10^{-5}	430
B	0.0009	0.0009	100
C	0.0187	0.0049	26
D	0.0327	0.0055	17
E	0.0543	0.0064	12
F	0.0779	0.0074	10

It remains to be determined how many repeated runs are needed to give an accurate estimate of uncertainty. For the 6 pixels used here, 100 runs gave a relative uncertainty consistent to within 3-4%, and a mean glint within about 3% of the reported value, 1000 runs gave consistency in the uncertainty to 2-3% and a mean within 1% of the reported value. 10000 runs gave more reliable results, but may be too demanding of computation time for practical use. Note that consistency was much worse for the low glint values, but this should not matter for values below the medium glint threshold.

In general the mean values tended to be higher than that calculated from the mean values of the inputs: the function output for a random input is not normally distributed. This may mean that standard deviation is not the best measure of uncertainty for this data – interquartile range, as shown in [Figure 5](#), is a possible alternative.

Note on the sun glint calculation function

The function used to predict glint can rise to unrealistically high values for some input values - the PDF is well over 1. This is not physically realistic, however, in the MERIS method such pixels will fall in the high glint region so will not be corrected. An alternative is to use the Gaussian PDF instead of the Gram-Charlier expansion as currently used for SeaWiFS; [Figure 6](#) shows the range of values found for the MERIS function while [Figure 7](#) shows the range with a Gaussian PDF. Since OLCI is tilted, which reduces the glint, it's unlikely to be a problem because the highest glint conditions should not be encountered.



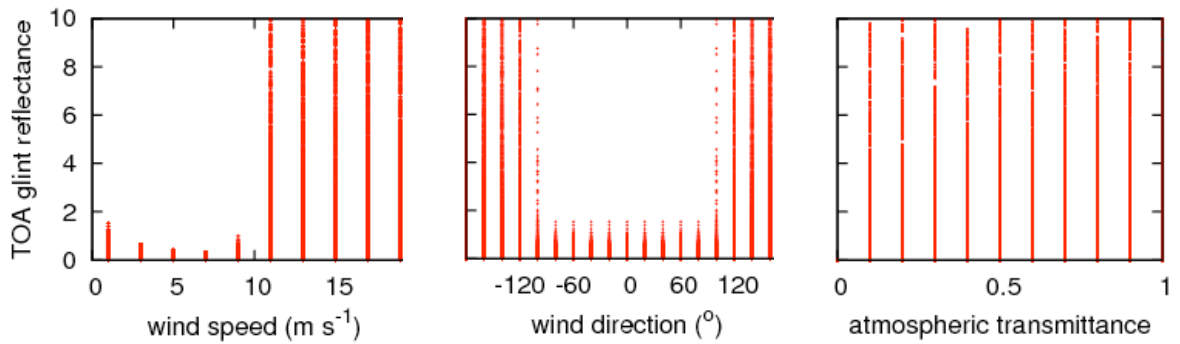


Figure 6: Top of atmosphere glint reflectance calculated for values across the full range of all input variables, plotted against each variable. Note that points with values of glint reflectance above 10 are not shown.

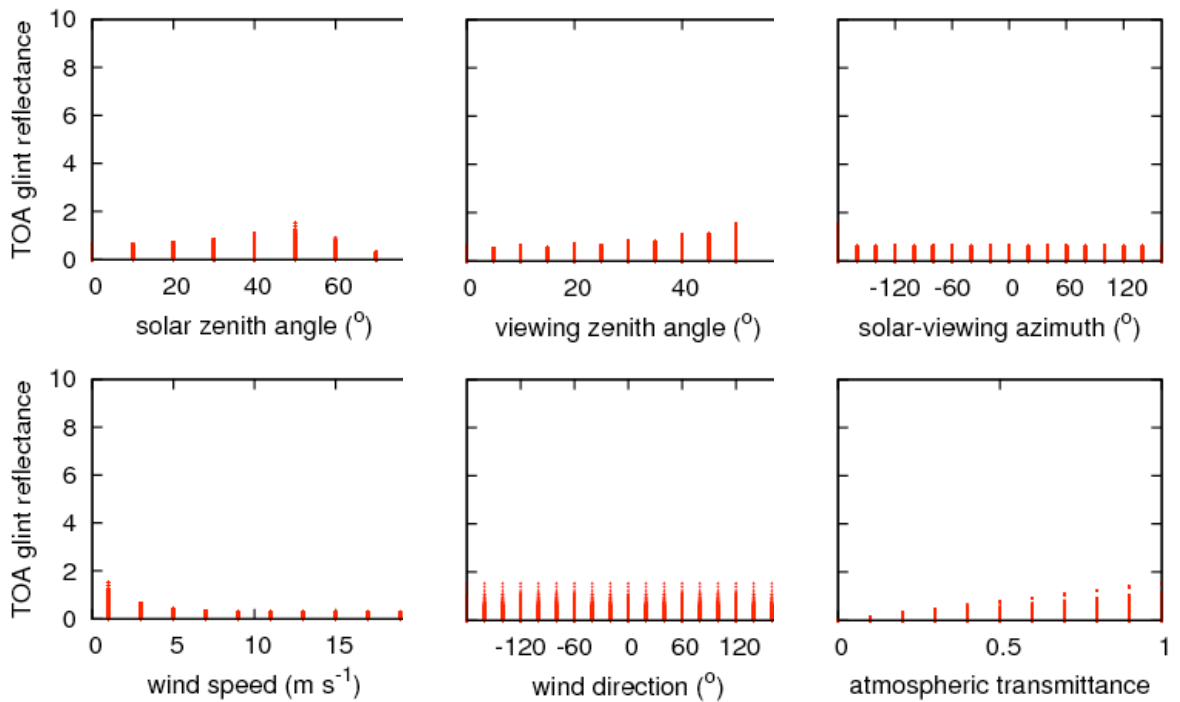


Figure 7: Top of atmosphere glint reflectance calculated for values across the full range of all input variables, plotted against each variable using the Gaussian PDF version of the glint function.

	<p style="text-align: center;">SENTINEL-3 OPTICAL PRODUCTS AND ALGORITHM DEFINITION</p> <p style="text-align: center;">OLCI Level 2 ATBD Glint Correction</p>	<p>Ref: S3-L2-SD-03-C09-ARG- ATBD Issue: 2.1 Date: 11/10/2012 Page 19 of 24</p>
---	--	---

4. PRACTICAL CONSIDERATIONS / EVOLUTION

The function (equation 4) is not well behaved for all input values. The expansion with the c_{21} , c_{03} etc. can become negative, giving a positive argument for $\exp()$. This is not physically realistic, but won't matter if the reflectance is only used for thresholds – these values would be calculated as 'high glint' and the pixels left uncorrected. In the NASA implementation (within SeaDAS) this full expansion is not used - just a Gaussian PDF – but the full expression is more accurate for some seas.

The Cox and Munk model has the limitation that the wind data may not have sufficient resolution to capture the effects of local winds, and it doesn't include the effects of atmospheric stability, wind age or swell (Hwang 2008; Hwang and Shemdin, 1988; Shaw and Churnside 1997). Kay et al. (Submitted) is working on the feasibility of Monte Carlo modelling of very high resolution surface models that incorporate slope and elevation features on scales from millimetres to tens of metres. The current approach validates well against a Cox and Munk slope statistics model, but displays small differences at non-orthogonal reflectance directions. Preliminary results also indicate that that recent developments in spreading function models may have optical consequences of relevance, at least to off-nadir viewing sensors.

In the baseline implementation the diffuse transmittance does not include the aerosol optical thickness because otherwise it would require an iterative loop. This iterative loop is currently implemented within the SeaDAS code for MODIS/SeaWiFS processing, but at this stage it's unclear whether Near real-time (NRT) products shall be delivered to the users in less than 3 hours after acquisition which could place a constraint on the complexity of the processor. An alternative to an iterative loop would be to set a climatological aerosol optical thickness value where an underestimation is envisaged as the atmospheric correction itself will be able to partly correct for sun glint, see Figure 3 as an example using CASI (airborne) image processing using an atmospheric correction as described by Lavender and Nagur (2002). The uncorrected image shows a significant variation in brightness across the image caused by sun glint (Figure 8a). The land was successfully removed by the non-water mask, but the sun glint affected (left hand side) water pixels were also masked (Figure 8b). Therefore, the mask was switched off for the further processing, which demonstrated that spurious results were created on the land, but that the atmospheric correction worked over the sun glint influenced area (see Figure 8c to 3d). The bio-optics model (Pinkerton et al. 2006) did produce a plausible Total Suspended Matter (TSM) image, but was influenced by the sun glint and shows significantly lower TSM values in the affected area.

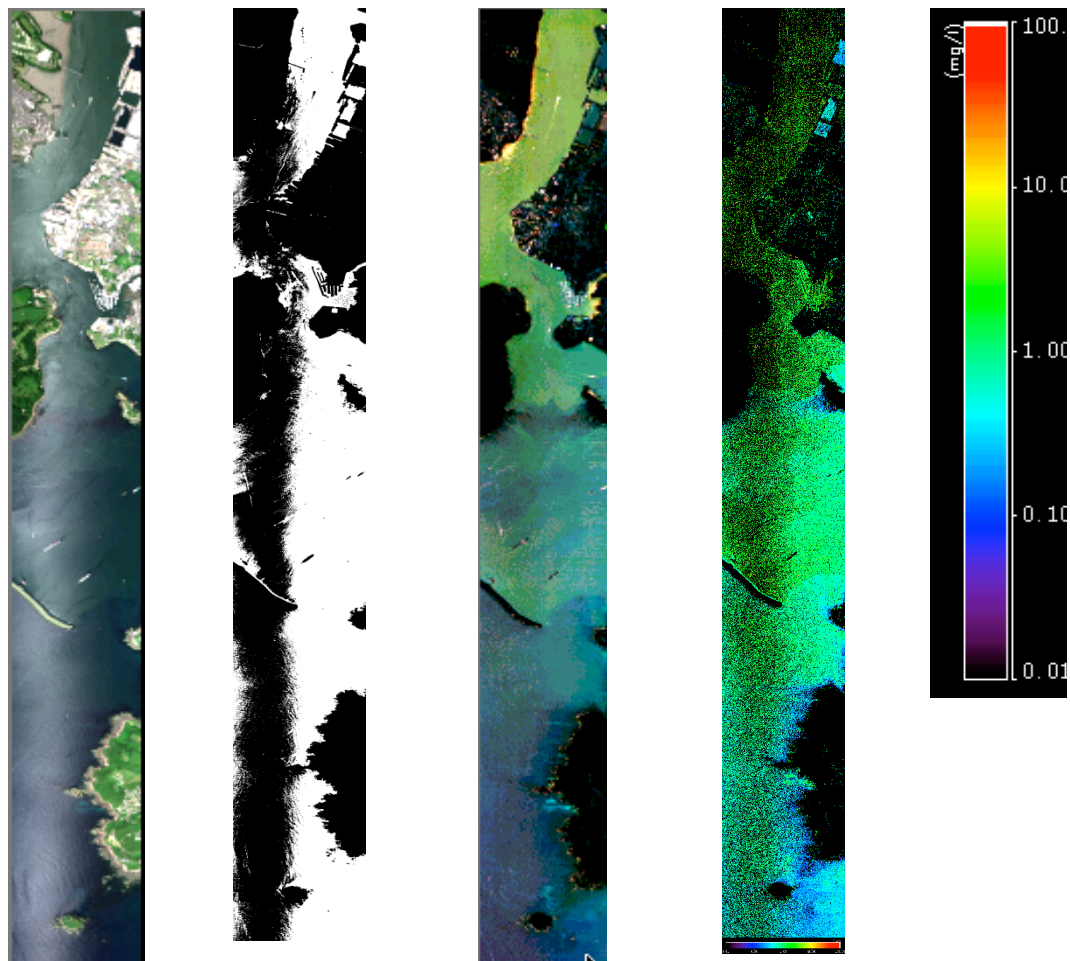


Figure 8: CASI imagery for the 13 June 2003 flown over the Tamar Estuary and Plymouth Sound, UK. The quasi true coloured images (a and c) represent composites of wavebands centred at 672, 561 and 491 nm as red, green and blue. From left to right the images are uncorrected image, non-water mask, aerosol corrected image and TSM product with the scale bar.

	<p style="text-align: center;">SENTINEL-3 OPTICAL PRODUCTS AND ALGORITHM DEFINITION</p> <p style="text-align: center;">OLCI Level 2 ATBD Glint Correction</p>	<p>Ref: S3-L2-SD-03-C09-ARG- ATBD Issue: 2.1 Date: 11/10/2012 Page 21 of 24</p>
---	--	---

5.

6. ASSUMPTIONS AND LIMITATIONS

Current RT models include a limited number of processes, and there is scope to improve the models by building in multiple scattering, polarization, multiple reflections at the water surface and the shadowing effects of large waves. Glint and atmospheric correction are intimately linked, and it's likely that future approaches will use RT modelling to do both corrections together. Therefore, two approaches will be implemented in the level 2 processor:

- Current MERIS approach as the baseline (this ATBD)
- Neural Network as an alternative approach (ATBD SD-03-C17)

Current algorithms also use the Cox and Munk (1954a,b) model of the sea surface and the effect of using more recent models can also be explored.

7. INPUT DATA

Diffuse transmittance: t_d [dimensionless]

Geometry including illumination and viewing zenith and azimuth angles: θ_s [degrees], θ_v [degrees] and $\Delta\phi$ [degrees]

Wind speed: W [m/s]

	<p style="text-align: center;">SENTINEL-3 OPTICAL PRODUCTS AND ALGORITHM DEFINITION</p> <p style="text-align: center;">OLCI Level 2 ATBD Glint Correction</p>	<p>Ref: S3-L2-SD-03-C09-ARG- ATBD Issue: 2.1 Date: 11/10/2012 Page 22 of 24</p>
---	--	---

8. REFERENCES

ACRI, 2006. MERIS Level 2 Detailed Processing Model. Available at: http://earth.esa.int/pub/ESA_DOC/ENVISAT/MERIS/MERIS_DPML2_i7r2A_re-issued.pdf

Bréon, F. and Henriot, N. 2006. Spaceborne Observations of Ocean Glint Reflectance and Modeling of Wave Slope Distributions. *J. Geophys. Res.*, 111, C06005:1- C06005:10.

Cox, C. and Munk, W. 1954a. Measurement of the Roughness of the Sea Surface from Photographs of the Sun's Glitter. *Journal of the Optical Society of America*, 44(11), pp 838-850.

Cox, C. and Munk, W. 1954b. Statistics of the Sea Surface Derived from Sun Glitter. *Journal of Marine Research*, 13(2), pp 198-227.

Cox, C. and Munk, W. 1956. Slopes of the sea surface deduced from photographs of sun glitter. *Scripps Institute of Oceanography Bulletin*, 6(9), pp 401-488.

Doerffer, R. et al., 2008. The impact of sun glint on the retrieval of water parameters and possibilities for the correction of MERIS scenes. Available at: <http://earth.esa.int/cgi-bin/confm8.pl?abstract=201>.

Ebuchi, N. and Kizu, S. 2002. Probability Distribution of Surface Wave Slope Derived Using Sun Glitter Images from Geostationary Meteorological Satellite and Surface Vector Winds from Scatterometers. *Journal of Oceanography*, 58(3), pp 477-486.

Fox, D. et al., 2007. Near-surface wind speed retrieval from space-based, multi-angle imaging of ocean sun glint patterns. *Remote Sensing of Environment*, 107(1-2), pp 223-231.

Fukushima, H. et al. 2007. Evaluation of ADEOS-II GLI ocean color atmospheric correction using SIMBADA handheld radiometer data. *Journal of Oceanography*, 63(3), pp 533-543.

Fukushima, H. et al., 2009. Improvement of the ADEOS-II/GLI sun-glint algorithm using concomitant microwave scatterometer-derived wind data. *Advances in Space Research*, 43(6), pp 941-947.

Gatebe, C. et al. 2005. Airborne spectral measurements of ocean directional reflectance. *Journal of the Atmospheric Sciences*, 62(4), pp 1072-1092.

	<p style="text-align: center;">SENTINEL-3 OPTICAL PRODUCTS AND ALGORITHM DEFINITION</p> <p style="text-align: center;">OLCI Level 2 ATBD Glint Correction</p>	<p>Ref: S3-L2-SD-03-C09-ARG- ATBD Issue: 2.1 Date: 11/10/2012 Page 23 of 24</p>
---	--	---

Helton, J. et al., 2006. Survey of sampling-based methods for uncertainty and sensitivity analysis. *Reliability Engineering & System Safety*, 91(10-11), 1175-1209.

Hwang, P.A. 2008. Observations of Swell Influence on Ocean Surface Roughness. *J. Geophys. Res.*, 113, C12024:1- C12024:14.

Hwang, P. and Shemdin, O. 1988. The Dependence of Sea-Surface Slope on Atmospheric Stability and Swell Conditions. *J. Geophys. Res.*, 93, 13903-13912.

Kay, S., Hedley, J.D. and Lavender, S. 2009. Sun Glint Correction of High and Low Spatial Resolution Images of Aquatic Scenes: a Review of Methods for Visible and Near-infrared Wavelengths. *Remote Sensing*, Vol. 1, Issue 4, 697-730.

Kay, S. et al. Submitted. Modeling the transfer of light at the ocean surface: an approach based on high-resolution surface wave models. *Ocean Optics OOX*, submitted extended abstract.

Lavender, S.J. and Nagur, C.R.C. 2002. Mapping UK coastal waters with high resolution imagery. *Journal of Optics A: Pure and Applied Optics*, Vol. 4, S50-S55.

Montagner, F., Billat, V. and Belanger, S. 2003. MERIS ATBD 2.13 Sun Glint Flag Algorithm. Available at: http://envisat.esa.int/instruments/meris/atbd/atbd_2_13.pdf.

Ottaviani, M. et al. 2008. Improving the description of sunglint for accurate prediction of remotely sensed radiances. *Journal of Quantitative Spectroscopy & Radiative Transfer*, 109(14), pp 2364-2375.

Pinkerton, M.H., Moore, G.F., Lavender, S.J., Gall, M.P., Oubelkheir, K., Richardson, K.M., Boyd, P.W. and Aiken, J. 2006. A method for estimating inherent optical properties of New Zealand continental shelf waters from satellite ocean colour measurements. *New Zealand Journal of Marine and Freshwater Research*, 40, 227–247.

Saltelli, A. et al., 2006. Sensitivity analysis practices: Strategies for model-based inference. *Reliability Engineering & System Safety*, 91(10-11), 1109-1125.

Shaw, J. and Churnside, J. 1997. Scanning-Laser Glint Measurements of Sea-Surface Slope Statistics. *Appl. Opt.*, 36, 4202-4213.

Steinmetz, F., Deschamps, P. and Ramon, D. 2008. Atmospheric correction in presence of sunglint: application to MERIS. Available at: <http://earth.esa.int/cgi-bin/confm8.pl?abstract=75>.

	<p style="text-align: center;">SENTINEL-3 OPTICAL PRODUCTS AND ALGORITHM DEFINITION</p> <p style="text-align: center;">OLCI Level 2 ATBD Glint Correction</p>	<p>Ref: S3-L2-SD-03-C09-ARG- ATBD Issue: 2.1 Date: 11/10/2012 Page 24 of 24</p>
---	--	---

Wang, M. and Bailey, S. 2001. Correction of sun glint contamination on the SeaWiFS ocean and atmosphere products. *Applied Optics*, 40(27), pp 4790-4798.

Wu, J. 1990. Mean-Square Slopes of the Wind-Disturbed Water-Surface, Their Magnitude, Directionality, and Composition. *Radio Science*, 25(1), pp 37-48.

Wang, M. et al. 2002. Ocean-color optical property data derived from the Japanese ocean color and temperature scanner and the French polarization and directionality of the earth's reflectances: a comparison study. *Applied Optics*, 41(6), pp 974-990.

ACKNOWLEDGEMENTS

Natural Environment Research Council (NERC) small grant (NER/B/S/2002/00555, PI Lavender) and the NERC Airborne Research and Survey Facility supported the CASI work. Susan Kay's PhD work is part of a project supported by ARGANS Ltd and Great Western Research